Sc_2C, a 2D semiconducting electride

Lauren M. McRae†, Rebecca C. Radomsky†, Jacob T. Pawlik†, Daniel L. Druffel†, Jack D. Sundberg†, Matthew G. Lanetti†, Carrie L. Donley‡, Kelly L. White†, and Scott C. Warren*,†

†Department of Chemistry, University of North Carolina at Chapel Hill, Chapel Hill, North Carolina 27599, United States

‡Chapel Hill Analytical and Nanofabrication Laboratory (CHANL), University of North Carolina at Chapel Hill, Chapel Hill, North Carolina 27599, United States

ABSTRACT: Electrides are exotic materials that typically have electrons present in well-defined lattice sites rather than within atoms. Although all known electrides have an electropositive metal cation adjacent to the electride site, the effect of cation electronegativity on the properties of electrides is not yet known. Here, we examine trivalent metal carbides with varying degrees of electronegativity and experimentally synthesize Sc_2C. Our studies identify the material as a 2D electride, even though Sc is more electronegative than any metal previously found adjacent to an electride site. Further, by exploring Sc_2C and Al_2C computationally, we find that higher electronegativity of the cation drives greater hybridization between metal and electride orbitals, which opens a band gap in these materials. Sc_2C is the first 2D electride semiconductor, and we propose a design rule that cation electronegativity drives the change in band structure.

INTRODUCTION

Challenges in energy storage, electronics, and catalysis motivate the search for exotic materials with extreme properties, and electrides—crystals with bare electrons trapped at stoichiometric concentrations[1–3]—offer some of the most exceptional. These electrons have been ejected from atomic orbitals to reside in vacant lattice sites and, because they are so weakly bound, are better electron donors than alkali metals[4–6], can offer electrical conductivity that rivals silver[6], and can catalyze challenging reactions[6]. These properties have led to the exploration of electrides in applications where electron-rich materials are needed: N_2 and CO_2 reduction[7,8], battery electrodes[9,10], and electron emitters[11–13]. Despite this progress, rules that might predict an electride's properties based on its structure or composition are underdeveloped. For example, unlike in conventional materials, it is not known how to tune the band gap of electrides. And, even more critically, simple rules that could predict whether a material is an electride remain imprecise[3,14].

Presently, just two rules for predicting electrides are widely accepted: (1) the metal atoms that form the coordination sphere around the electride electron must be electropositive[15], and (2) the compound must be electron rich[16]. For example, in $[Ca_2N]^+(e^-)$[17], calcium is electropositive, and the compound is electron rich because the preferred oxidation states (Ca^{2+}, N^{3-}) and stoichiometry provide an extra electron, forming an electride. These rules are far too broad, however, because many compounds fulfill these rules but are not electrides.

To improve these rules, experiments have begun to identify the metals that can be adjacent to an electride electron. So far, only Ca[5], Sr[18,19], Ba[17,20], Y[21,22], Hf[23], and Gd[24,25] have been incorporated next to the electride site (Figure 1), while Sc and several of the lanthanide series have been identified as candidates computationally[26,27,28]. This delicate balance between electron counting and electronegativity was recently explored in the case of Ca_5Pb_3 (not an electride) and $Ca_3Hf_2Pb_3$ (an electride), as replacing calcium for hafnium makes the compound electron rich[16]. Despite these findings, the limit of cation electronegativity in the formation of electrides is not yet known. Therefore, to develop improved design rules for electrides and for their structure-property relationships, we explore the trivalent metal carbides with a layered structure. This family is informative because Y_2C is a known electride[22], Sc_2C has been predicted[26], and Al_2C is unknown, and further, these metals vary systematically in electronegativity (Figure 1).

The question of electronegativity is essential because two experimentally observed electrides—Y_2C and Hf_2S—are "hybrid" electrides[3], where the electride electron has some overlap with the adjacent metal orbitals, and electronegativity of the metal may be correlated with the degree of hybridization. This covalency plays an important role in defining the

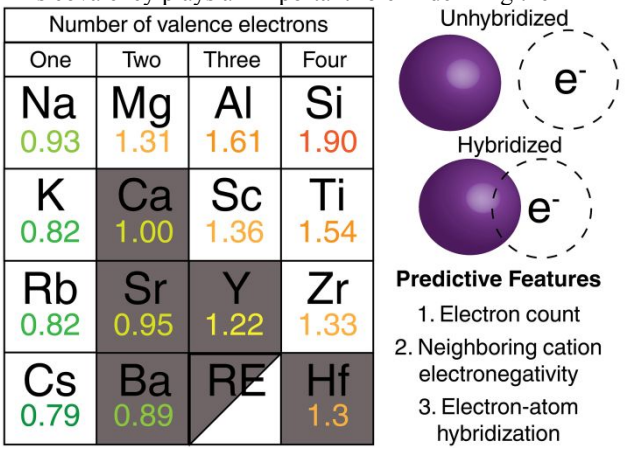

Figure 1. An adapted periodic table highlighting the valency of various cations. The Pauling electronegativity values are shown beneath each element symbol, and the gray blocks indicate which cations have been experimentally incorporated next to an electride site. The predictive features for potential electrides are listed and electride electron-atom hybridization is illustrated.

electronic structure of the electride because the electride electron is normally found around the Fermi level. Thus, as hybridization occurs, tunable band structures become possible, and indeed, Y_2C is a semi-metal. While there are examples of 0D electrides[28-31] and electron-rich semiconductors[32,] this semi-metal character is unique among the 2D electrides[3,33]. This peculiarity raises the question of whether greater degrees of hybridization between metal and electride electron could lead to new categories of electride materials[34].These questions motivate our exploration of the M_2C system, and especially of layered Sc_2C.

To highlight uncertainties within the Sc_2C system, we briefly outline previous findings and predictions. Sc_2C was originally synthesized in 1967 and assigned to the NaCl structure type, which we refer to below as the cubic phase[35]. In 1969, different authors reassigned the structure as layered ($R\bar{3}m$) on the basis of its powder x-ray diffraction (PXRD) pattern[21,36], even though the pattern was missing several important reflections (Table S2). In 1989, the structure was again reassigned as the cubic phase[37] (Figure 2a, updated with our findings). This assignment appears to be correct and it is not known whether a layered Sc_2C electride exists. Currently, a 2D Sc_2C MXene structure has been explored computationally[38,39] and calculations predict that layered Sc_2C would be an electride[26]. In addition, 2D Sc_2C has been predicted to store an impressive 8% hydrogen by weight[40,41] and reversibly store fluoride as a battery anode at capacities that exceed state-of-the-art lithium-ion batteries[10]. Thus, if a layered Sc_2C electride does exist, it could allow these exciting predictions to be realized.

In this study, we predict that layered Sc_2C is stable using an evolutionary algorithm and experimentally explore the phase diagram around the desired composition. We then calculate the electronic structure of the synthesized material and compare it to Y_2C and Al_2C to understand periodic trends. We find that as the cation becomes more electronegative, the band gap opens with Y_2C as a semimetal, Sc_2C as a small band gap semiconductor, and Al_2C as a larger gap semiconductor. The synthesized layered Sc_2C is the first 2D electride with semiconducting properties, opening up a fascinating new class of electride materials with several possible applications in energy storage or optoelectronics.

RESULTS AND DISCUSSION

Phase diagram exploration

Although layered Sc_2C is unknown, we and Hirayama *et. al.*[26] have hypothesized that it exists because Sc is chemically similar to Y and layered Y_2C is a stable phase. To investigate whether layered Sc_2C is thermodynamically stable, we used USPEX to explore the scandium-carbon phase space. The phase diagram we obtained indicates that the Sc_2C composition is on the hull, and that the layered $R\bar{3}m$ structure is stable by 28 meV/atom (Figure 2b). This modest relative stability could suggest why the layered phase had not previously been synthesized.

The possibility that layered Sc_2C is thermodynamically stable motivated us to make this compound via high-temperature solid-state synthesis. In the Y_2C synthesis, we observed that high oxygen content in the yttrium led to formation of the cubic phase (YC_x). With this in mind, compared to the synthesis performed in Rassaerts *et. al.*'s 1967 study, we suspected that our use of high purity scandium with a lower oxygen content would allow us to experimentally realize our computational

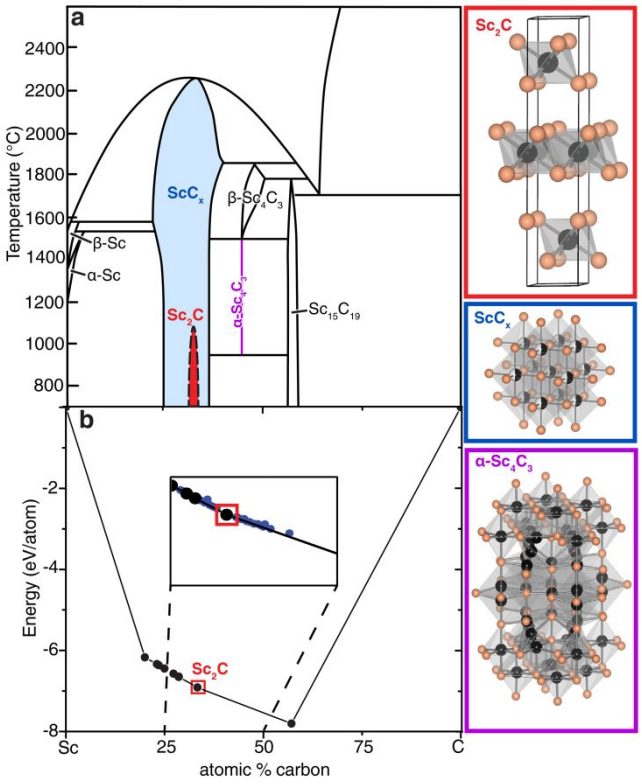

Figure 2. (a) The binary Sc-C phase diagram[37], including the layered Sc_2C phase (red). (b) The hull diagram for the Sc-C phase, as calculated with USPEX. The conventional unit cell for layered Sc_2C (red), cubic ScC_x (blue), and α-Sc_4C_3 (purple) are shown.

prediction. We arc-melted scandium and carbon in ratios from 2:0.9 to 2:1.15, respectively. These arc-melted samples had a high content of the cubic structure (ScC_x) (Figure S2), but arc-melting has a rapid cool-down, so the structure may not be at equilibrium. Therefore, we followed arc-melting with annealing for 7 days at 1100°C to increase the likelihood of observing the thermodynamically favored layered phase. We found that the cubic structure is stable both at compositions with deficient carbon (Figure S3) and excess carbon (Figure S4). However, at a composition of 2:0.99, the layered structure was observed, and this is reflected in the new binary phase diagram we propose for the Sc-C system (Figure 2a)[37]. There is uncertainty in the assignment of the temperature at which the congruent layered-to-cubic phase change occurs, but our experiments indicate that the layered phase is stable to at least 1100°C.

To fully understand the structure of the layered phase, we first performed PXRD experiments of the product at room temperature and refined the pattern using the Rietveld method[42] (Figure 3). The pattern indexed as the R$\bar{3}$m structure with lattice parameters of a = b = 3.337 Å and c = 16.346 Å. This refinement includes the incorporation of preferred orientation at {104} with a March coefficient of 0.754. The sample contained up to 15% of the cubic ScC_x, which we attribute to a relatively low stability of the layered phase as well as possible oxygen contamination in the Sc reactant. To quantitatively compare the predicted and experimental structures, we further optimized the structure from USPEX using the PBEsol functional. The calculated lattice parameters were 0.68% smaller in a and 0.09% smaller in c, which is within the typical error between PBEsol and

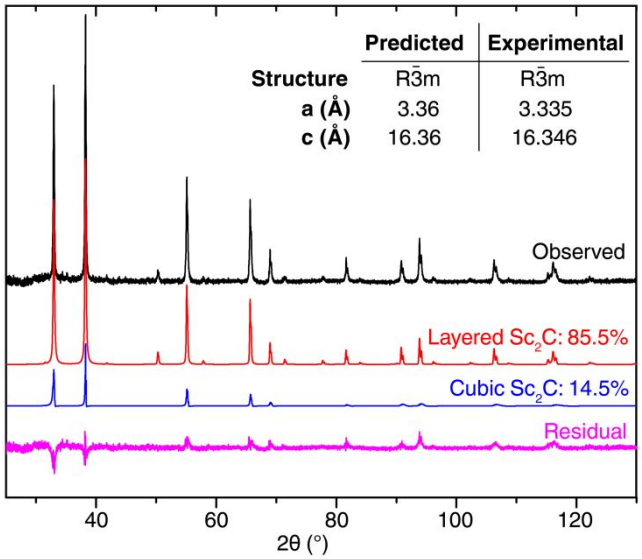

Figure 3. X-ray diffraction patterns of the experimental structure compared to the calculated layered and cubic Sc_2C phases. The calculated amounts of the layered and cubic are shown as determined by the Rietveld method. The predicted and experimental lattice parameters are compared.

experiment. This further confirms that the synthesized material is layered Sc_2C.

To better understand the effect of annealing in these samples, we obtained high-resolution transmission electron microscopy (HRTEM) of the product at room temperature under high vacuum. In Figure 4, we compare the Fast Fourier Transform (FFT) of these samples, where the non-annealed sample shows a ring pattern while the annealed sample shows well-defined spots. From the FFT images, we constructed filtered HRTEM images to create a color-coded map of crystalline domains where we compare the crystallinity of Sc_2C before and after annealing. The filtered HRTEM images and FFTs confirm that the domain size is small prior to annealing, likely due to kinetic trapping from rapid cooling after arc-melting. Even with annealing, there was still about 15% of the cubic phase present, which we attribute to a small amount of oxygen in the sample. In an attempt to leach any oxygen present in the reaction container, we tried the synthesis in the presence of a titanium sponge. This did not improve the layered content of the sample. We, therefore, suspect that impurities in the product must come from impurities present in the Sc reactant. Specifically, Sc that is nominally 99.999% pure typically contains 0.1-0.5 at.% oxygen[43], thus favoring a small amount of the cubic phase.

In addition, we used TEM to confirm that the layered Sc_2C phase is dominant. While from XRD there is a small amount of cubic Sc_2C (14.5%) compared to layered Sc_2C (85.5%), the refinement has some uncertainty because the layered and cubic patterns are similar. In electron diffraction, the most common spatial frequency corresponds to a d-spacing of 2.3 Å, which we assign to either {104} in the layered structure or {101} in the cubic structure. This ambiguity motivated us to find distinct peaks for the layered phase. To identify the phase of these domains, we sought to acquire diffraction patterns containing the {117} reflection of the layered phase, which is expected at 5.501 nm^{-1}, for which there are no reflections in the cubic phase. In Figure 4c, we observe diffraction spots at 5.479 nm^{-1}, which can only be assigned to the layered phase. Simulations of the cubic structure with varied arrangements of carbon and carbon vacancies also failed to show a diffraction peak at 5.501 nm^{-1}. Importantly, the prevalence of {117} in diffraction patterns increases upon annealing, in agreement with XRD. In addition, XRD and TEM lattice spacings agree within 0.6%. This data confirms the experimental structure from XRD and corroborates the Rietveld refinement result.

Assessment of electride character and electronic structure

Having confirmed the existence of layered Sc_2C as a thermodynamically stable material, we examined the material's electride character. In the experimental structure determined from our Rietveld refinement, there was a longer scandium-scandium distance (3.53 Å) than in scandium metal (3.22 Å) and Sc_2O_3 (3.27 Å). This increased distance could indicate that electride electrons are present, so we sought evidence by calculating the electron localization function (ELF) using the hybrid DFT functional HSE-06. The ELF measures the degree of electron spatial localization compared to a reference electron with the same spin and provides a map of electron probability across a system. The ELF of Sc_2C shows localization of electrons that are not associated with either the scandium or carbon atoms, and indicates that there is electride character

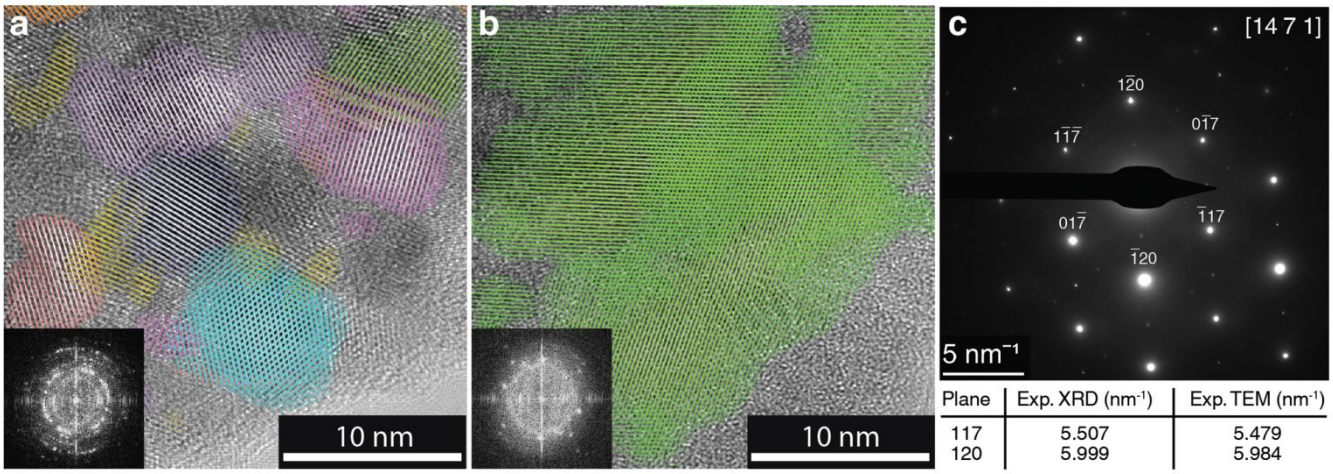

Figure 4. (a) A high-resolution TEM image of Sc_2C before annealing, with colored lattice planes corresponding to different crystallite regions determined through FFTs. (b) A high-resolution TEM image of Sc_2C after annealing for 7 days, with the lattice planes of the single crystallite region in green. (c) A selected area electron diffraction (SAED) pattern of the [14 7 1] zone axis. The corresponding experimental d-spacings are compared.

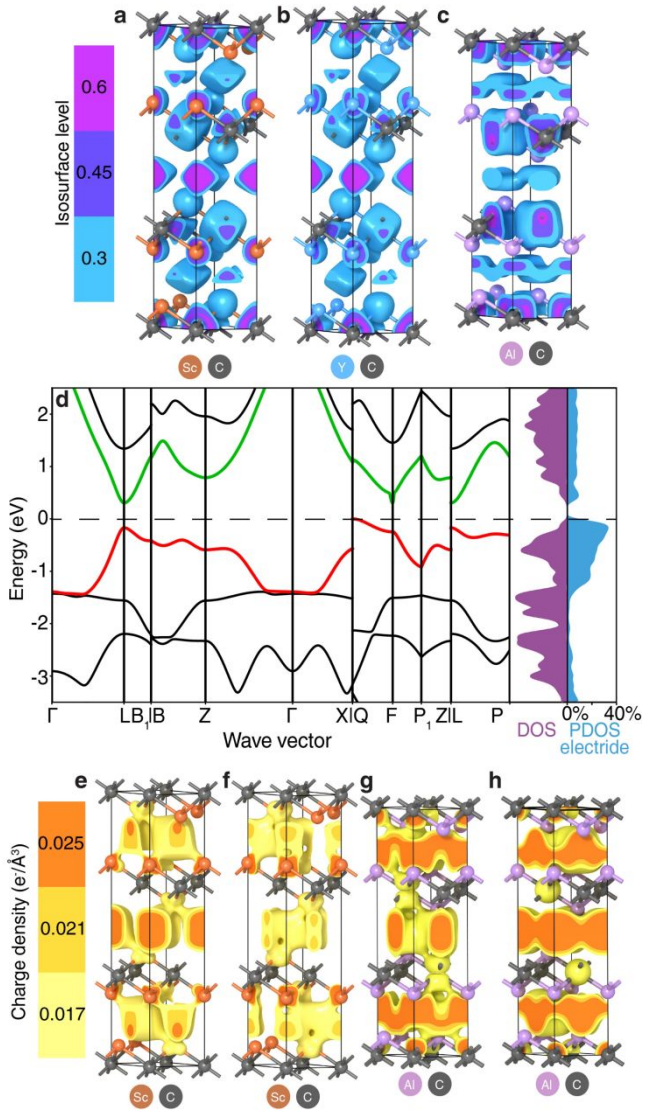

Figure 5. (a) The 3D ELF of Sc_2C, where the gradient of isosurface level spans from 0.3-0.6. This scale is the same for each ELF. (b) The 3D ELF of Y_2C. (c) The 3D ELF of Al_2C. (d) The Sc_2C band structure, total density of states (purple), and partial density of the electride states as a percentage of the total (blue). The valence and conduction bands are highlighted in red and green, respectively. (e) The charge density of the Sc_2C valence band at the L point. The gradient of charge density spans from 0.017 $e^-/Å^3$ - 0.025 $e^-/Å^3$. This scale is the same for each charge density. (f) The charge density of the Sc_2C conduction band at the L point. (g) The charge density of the Al_2C valence band at the L point. (h) The charge density of the Al_2C conduction band at the L point.

in the layered structure (Figure 5a).

We calculated the band structure and density of states (DOS) with HSE-06 and found that Sc_2C is a semi-conductor with a 0.305 eV indirect band gap and a 0.476 eV direct band gap (Figure 5d). We attempted to further purify Sc_2C, but the cubic phase remained in all experiments. This prevented us from making electrical and optical band gap measurements on pure layered Sc_2C.

Emergence of semiconducting behavior in electrides

To understand how cation electronegativity plays a role in band structure, we compare these results to the electronic structure of Y_2C and Al_2C. The known hybrid electride Y_2C has a similar ELF to Sc_2C, where there is electron character that is not associated with either the yttrium or carbon atoms (Figure 5b). Yttrium has an electronegativity value of 1.22, whereas scandium has a value of 1.36[44]. Therefore, Sc_2C has the most electronegative metal adjacent to the electride site yet synthesized in a 2D electride. We wanted to further explore a possible electride structure with a similar, yet more electronegative metal, aluminum (1.61). The theoretical layered Al_2C has the same structure type as Y_2C and Sc_2C, but there is less observed electron localization in this structure between the layers of Al_2C (Figure 5c). We calculated band structures and band gaps of Y_2C (Figure S5), Sc_2C (Figure 5d), and Al_2C (Figure S6) using the same calculation parameters. Although Y_2C is a semimetal, we find that Sc_2C and Al_2C are indirect band gap semiconductors. In these systems, increasing cation electronegativity (Y to Sc to Al) correlates with an increasing band gap (0 to 0.31 to 0.50 eV, respectively).

From these observations, we propose a model in which increasing electronegativity of metal leads to increased hybridization. As electronegativity of the metal increases, unoccupied states lower in energy and become closer in energy to the occupied electride states. Because the metal and electride states are close in energy and can physically overlap, the states hybridize. The consequence of this hybridization is that the bonding states are stabilized and adopt some character of the metal orbitals while the anti-bonding states are destabilized and adopt some character of the electride orbitals (Figure S1). Thus, increasing metal electronegativity leads to increasing hybridization and a larger splitting between occupied and unoccupied states—i.e., the band gap increases.

If this model is correct, we should observe electride character in both the valence and conduction bands. Thus, we examined a partial density of electride states (Figure 5d) by integrating the charge within a sphere (radius = 1.2Å) centered at the electride lattice site. Although the hybridization leads to some Sc character in the integration, we observe the expected contributions of electride character near the top of the valence band and bottom of the conduction band. To better assess these states, we visualized charge density at the top of the valence band and bottom of the conduction band in Sc_2C and Al_2C (Figure 5e-h). This indeed revealed electride character in both bands, which could only result from hybridization of the electride electron and empty metal orbitals. This hybridization is analogous to a donor-acceptor interactions[47], such as BH_3-NH_3, but with the 2D electron layer playing the role of the donor and the 2D M_2C atoms playing the role of acceptor. Therefore, as overlap increases between donor (electride electrons) and acceptor (empty metal-carbide orbitals), the valence and conduction bands split more, and the band gap increases. Presumably, the greatest hybridization seen in the Al_2C system is facilitated by aluminum being most electronegative, since the empty Al orbitals are closer in energy to the electride electrons. Additionally, this model is supported by the observation that Al_2C's electride shows lower localization than Sc_2C (Figure 5a,c), which would be a consequence of this hybridization. These observations and model directly lead us to a powerful design rule for layered semiconducting electrides: that increasing metal electronegativity leads to increased electron-metal hybridization, yielding an increased band gap.

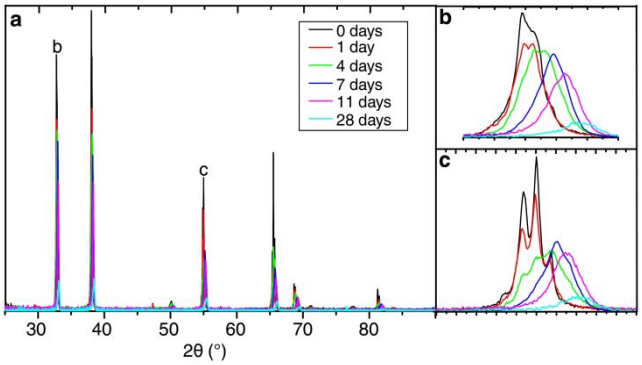

Figure 6. (a) X-ray diffraction patterns after various amounts of oxidation. (b) The diffraction pattern zoomed in between 54-56° two-theta. (c) The diffraction pattern zoomed in between 32.4-33.4° two-theta.

Exfoliation potential

To explore the possibility of exfoliating layered Sc_2C to make the Sc_2C electrene, we calculated the energy to separate two monolayers of Sc_2C. We obtained a value of 2.76 J/m^2, which is larger than that of Y_2C[46]. Compared to other known layered electrides with similar structures (Ca_2N and Sr_2N), Sc_2C and Y_2C exhibit a similar trend wherein the electride with the smaller cation has a larger binding energy. This is likely due to the smaller cation naturally having a greater electrostatic attraction due to the smaller distance between opposite charges.

We also examined the mechanical properties of Sc_2C and Y_2C, since these properties are known to predict the exfoliation potential of a material[47]. We found that Sc_2C has a higher bulk modulus than Y_2C, while its shear modulus and Young's modulus are both lower (Table S6). The higher bulk modulus and lower shear modulus indicate that the material has a higher exfoliation potential than Y_2C. We explored this experimentally, but found that the material wouldn't exfoliate after sonicating in 1,3-dioxolane for 800 minutes[48]. SAED patterns and TEM images show that the particles that were produced were thick and irregularly shaped (Figure S10). Nevertheless, experimental exfoliation could lead to the realization of many exciting applications proposed for 2D Sc_2C[40,41] and could facilitate its study as an MXene-like derivative.

Stability in air

We tested the stability of this novel material in air because electrides are good reducing agents. Indeed, our calculations[49] of Sc_2C's work function—3.78 eV on the (0001) plane (Figure S8)—suggested that it could be a good electron donor, although less so than Y_2C[22], which has a slightly smaller work function and is more electropositive.

To explore the material's reactivity, we performed PXRD experiments after letting micron-sized particles (Figure S10) sit in air for varying intervals of time (Figure 6). The data shows that the material oxidizes slowly, with almost no change after sitting in air for one day. However, after four days, we observe that diffraction peaks shift to higher angles with decreased intensity and increased width. These attributes indicate a decrease in crystallinity and the formation of an amorphous material, which is the dominant phase by the final timepoint. Thus, unlike Hf_2S, Sc_2C is not naturally self-passivating.

To better understand the mechanism of oxidation, we performed x-ray photoelectron spectroscopy (XPS). High-resolution scans of scandium and carbon were taken after 0, 1, and 11 days of sitting in air (Figure 7). Scandium shows four distinct doublets at the initial timepoint, indicating that several scandium species were initially present on the material's surface. Component A, Sc^{3+} [(50)], is likely due to surface oxidation during transfer into the XPS. Component B matches the value previously reported for Sc^{2+} [(51)]. Component C has peaks that lie between components A and B, suggesting that thisSc is in an environment that is between that of these two components. Component D has a small peak with a low binding energy, which may be attributed to either scandium or nitrogen. The carbon XPS spectra also reveals four species at the initial timepoint Components E and G are adventitious carbon and its oxidized counterpart, respectively[52]. Component F is likely the carbide of Sc_2C. This component has an extremely small binding energy compared to other known transition metal carbide species, which is not surprising from an electride[53]. Component H is likely an intermediate species as the carbide oxidizes.

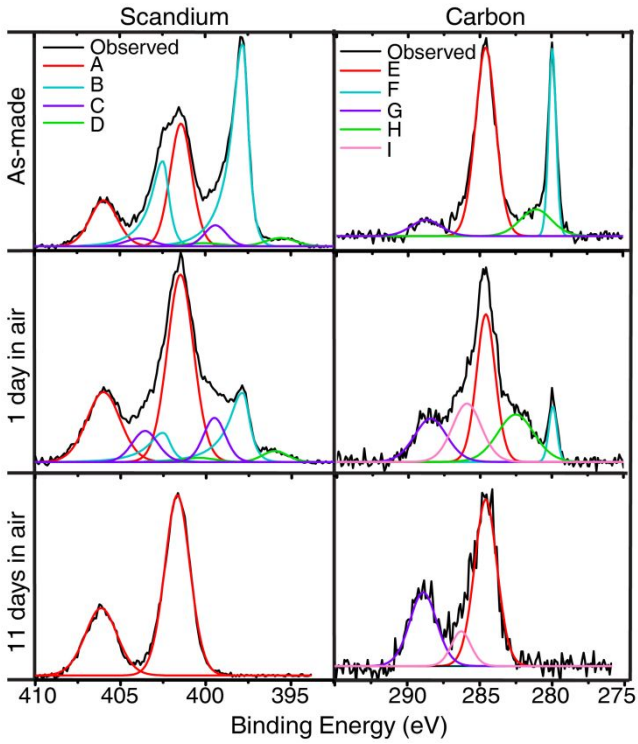

Figure 7. X-ray photoelectron spectroscopy spectra of scandium and carbon as-made, after 1 day in air, and after 11 days in air.

After one day of exposure to air, the Sc^{2+} peak decreases, the Sc^{3+} peak increases, and the carbide carbon peak decreases in intensity, indicating the sample is oxidizing. In the carbon spectra, a new species, component I, becomes apparent, and likely results from the adventitious carbon oxidizing. At the 11-day timepoint, the peaks associated with Sc_2C in both the scandium and carbon spectra have disappeared, indicating the surface was completely oxidized. The XRD data shows that there are still crystalline peaks present at the 11-day timepoint. From XRD and XPS, we conclude that an amorphous oxide forms on the surface of crystals first, and as the material continues to be exposed to air, oxygen diffuses further into the crystals until the bulk material becomes an amorphous oxide after 28 days. These results suggest that handling this material in air will require passivating coatings.

CONCLUSIONS

We have synthesized a new 2D inorganic electride, Sc_2C, which is the first semiconducting 2D electride. The discovery of this phase within the disordered rocksalt region of the Sc-C phase diagram suggests, in general, that other new electrides might be found within the rocksalt regions of many binary phase diagrams. Along with our exploration of Al_2C, the trivalent metal carbides lead to a new design rule for semiconducting 2D electrides: that more electronegative cations in 2D electrides lead to higher degrees of hybridization, resulting in greater splitting of valence and conduction bands. Therefore, based on the electronegativity of the cation, we predict that the band gap in these electride materials may be controllably tuned. This first example of a semiconducting 2D electride suggests possible applications as a catalyst or photocatalyst, where the already-excellent electron donating properties of the electride could be further enhanced by photoexcitation. In the case of Sc_2C, its small band gap specifically allows applications as an IR photodetector. These and other applications—e.g., in hydrogen storage[40,41] or as a fluoride ion battery electrode[10]—can now be experimentally explored.

ASSOCIATED CONTENT

Additional details regarding the literature search, computational and experimental methods, and experimental observations are included in the supporting information.

AUTHOR INFORMATION

Corresponding Author

Scott C. Warren- *Department of Chemistry, University of North Carolina at Chapel Hill, Chapel Hill, North Carolina, 27599, United States*
Email: sw@unc.edu

Authors

Lauren M. McRae- *Department of Chemistry, University of North Carolina at Chapel Hill, Chapel Hill, North Carolina, 27599, United States*
Rebecca C. Radomsky- *Department of Chemistry, University of North Carolina at Chapel Hill, Chapel Hill, North Carolina, 27599, United States*
Jacob T. Pawlik- *Department of Chemistry, University of North Carolina at Chapel Hill, Chapel Hill, North Carolina, 27599, United States*
Daniel L. Druffel- *Department of Chemistry, University of North Carolina at Chapel Hill, Chapel Hill, North Carolina, 27599, United States*
Jack D. Sundberg- *Department of Chemistry, University of North Carolina at Chapel Hill, Chapel Hill, North Carolina, 27599, United States*
Matthew G. Lanetti- *Department of Chemistry, University of North Carolina at Chapel Hill, Chapel Hill, North Carolina, 27599, United States*
Carrie L. Donley- *Chapel Hill Analytical and Nanofabrication Laboratory (CHANL), University of North Carolina at Chapel Hill, Chapel Hill, North Carolina, 27599, United States*
Kelly L. White- *Department of Chemistry, University of North Carolina at Chapel Hill, Chapel Hill, North Carolina, 27599, United States*

Author Contributions

The manuscript was written through contributions of all authors. All authors have given approval to the final version of the manuscript.

Funding Sources

This work was supported of this research by National Science Foundation under grant DMR-1905294. L.M.M. and R.C.R. acknowledge support by the NSF Graduate Research Fellowship (GRF) under grant DGE-1650116. J.T.P. and J.D.S acknowledge support by the NSF GRF under grant DGE-1650114. M.G.L. acknowledges support by the Department of Defense (DoD) through the National Defense Science & Engineering Graduate Fellowship (NDSEG). This work was performed in part at the Chapel Hill Analytical and Nanofabrication Laboratory, CHANL, a member of the North Carolina Research Triangle Nanotechnology Network, RTNN, which is supported by the National Science Foundation, Grant ECCS-2025064, as part of the National Nanotechnology Coordinated Infrastructure, NNCI.

Notes

The authors declare no competing financial interests.

ACKNOWLEDGMENT

Computational resources were provided, in part, by the Research Computing Center at the University of North Carolina at Chapel Hill. We acknowledge Dylan Storan for his insights on conductivity measurements. We acknowledge Dr. Renato Sampaio for his insights on optical band gap measurements.

REFERENCES

(1) Matsuishi, S., Toda, Y., Miyakawa, M., Hayashi, K., Kamiya, T., Hirano, M., Tanaka, I., Hosono, H. High-Density Electron Anions in a Nanoporous Single Crystal: $[Ca_{24}Al_{28}O_{64}]^{4+}(4e^-)$. *Science* **2003**, *301*, 626–630.

(2) Dye, J. L. Electrides: Early Examples of Quantum Confinement. *Acc. Chem. Res.* **2009**, *42*, 1564–1572.

(3) Hosono, H., Kitano, M. Advances in Materials and Applications of Inorganic Electrides. *Chem. Rev.* **2021**, *121*, 3121-3185.

(4) Toda, Y., Yanagi, H., Ikenaga, E., Kim, J. J., Kobata, M., Ueda, S., Kamiya, T., Hirano, M., Kobayashi, K., Hosono, H. Work Function of a Room-Temperature, Stable Electride $[Ca_{24}Al_{28}O_{64}]^{4+}(4e^-)$ 4. *Adv. Mater.* **2007**, *19*, 3564–3569.

(5) Gregory, D. H., Bowman, A., Baker, C. F., Weston, D. P. Dicalcium Nitride, Ca_2N - A 2D "excess Electron" Compound; Synthetic Rotates and Crystal Chemistry. *J. Mater. Chem.* **2000**, *10*, 1635–1641.

(6) Zhang, X., Yang, G. Recent Advances and Applications of Inorganic Electrides. *J. Phys. Chem. Lett.* **2020**, *11*, 3841–3852.

(7) Kuganathan, N., Hosono, H., Shluger, A. L., Sushko, P. V. Enhanced N_2 Dissociation on Ru-Loaded Inorganic Electride. *J. Am. Chem. Soc.* **2014**, *136*, 2216–2219.

(8) Qi, M., Tang, C., Zhou, Z., Ma, F., Mo, Y. Electride-Sponsored Radical-Controlled CO_2 Reduction to Organic Acids: A Computational Design. *Chem. - A Eur. J.* **2020**, *26*, 6234–6239.

(9) Hu, J., Xu, B., Yang, S. A., Guan, S., Ouyang, C., Yao, Y. 2D Electrides as Promising Anode Materials for Na-Ion Batteries from First-Principles Study. *ACS Appl. Mater. Interfaces* **2015**, *7*, 24016–24022.

(10) Druffel, D. L., Pawlik, J. T., Sundberg, J. D., McRae, L. M., Lanetti, M. G., Warren, S. C. First-Principles Prediction of Electrochemical Electron–Anion Exchange: Ion Insertion without Redox. *J. Phys. Chem. Lett.* **2020**, *1*, 9210–9214.

(11) Toda, Y., Matsuishi, S., Hayashi, K., Ueda, K., Kamiya, T., Hirano, M., Hosono, H. Field Emission of Electron Anions Clathrated

in Subnanometer-Sized Cages in $[Ca_{24}Al_{28}O_{64}]^{4+}(4e^-)$. *Adv. Mater.* **2004**, *16*, 685–689.

(12) Hosono, H., Hayashi, K., Kamiya, T., Atou, T., Susaki, T. New Functionalities in Abundant Element Oxides: Ubiquitous Element Strategy. *Sci. Technol. Adv. Mater.* **2011**, *12*, 034303.

(13) Menamparambath, M. M., Park, J. H., Yoo, H. S., Patole, S. P., Yoo, J. B., Kim, S. W., Baik, S. Large Work Function Difference Driven Electron Transfer from Electrides to Single-Walled Carbon Nanotubes. *Nanoscale* **2014**, *6*, 8844–8851.

(14) Dale, S. G., Johnson, E. R. Theoretical Descriptors of Electrides. *J. Phys. Chem. A* **2018**, *122*, 9371–9391.

(15) Redko, M. Y., Jackson, J. E., Huang, R. H., Dye, J. L. Design and Synthesis of a Thermally Stable Organic Electride. *J. Am. Chem. Soc.* **2005**, *127*, 12416–12422.

(16) Li, K., Gong, Y., Wang, J., Hosono, H. Electron-Deficient-Type Electride Ca_5Pb_3: Extension of Electride Chemical Space. *J. Am. Chem. Soc.* **2021**, *143*, 8821–8828.

(17) Walsh, A., Scanlon, D. O. Electron Excess in Alkaline Earth Sub-Nitrides: 2D Electron Gas or 3D Electride? *J. Mater. Chem. C* **2013**, *1*, 3525–3528.

(18) Brese, N. E., O'Keeffe, M. Synthesis, Crystal and Physical Properties of Sr_2N. *J. Solid State Chem.* **1990**, *87*, 134–140.

(19) Chanhom, P., Fritz, K. E., Burton, L. A., Kloppenburg, J., Filinchuk, Y., Senyshyn, A., Wang, M., Feng, Z., Insin, N., Suntivich, J., *et al.* Sr_3CrN_3: A New Electride with a Partially Filled d-Shell Transition Metal. *J. Am. Chem. Soc.* **2019**, *141*, 10595–10598.

(20) Reckeweg, O., DiSalvo, F. J. Crystal Structure of Dibarium Mononitride, Ba_2N, an Alkaline Earth Metal Subnitride. *Zeitschrift fur Krist. - New Cryst. Struct.* **2005**, *220*, 549–550.

(21) Atoji, M., Kikuchi, M. Crystal Structures of Cubic and Trigonal Yttrium Hypocarbides; A Dimorphically Interphased Single-Crystal Study. *J. Chem. Phys.* **1969**, *51*, 3863–3872.

(22) Zhang, X., Xiao, Z., Lei, H., Toda, Y., Matsuishi, S., Kamiya, T., Ueda, S., Hosono, H. Two-Dimensional Transition-Metal Electride Y_2C. *Chem. Mater.* **2014**, *26*, 6638–6643.

(23) Kang, S. H., Kang, S. H., Bang, J., Chung, K., Nandadasa, C. N., Han, G., Lee, S., Lee, K. H., Lee, K., Ma, Y., *et al.* Water- And Acid-Stable Self-Passivated Dihafnium Sulfide Electride and Its Persistent Electrocatalytic Reaction. *Sci. Adv.* **2020**, *6*. 4819-4835.

(24) Mudryk, Y., Paudyal, D., Pecharsky, V. K., Gschneidner, K. A. Magnetic Properties of Gd_2C: Experiment and First Principles Calculations. *J. Appl. Phys.* **2011**, *109*, 2–5.

(25) Lee, S. Y., Hwang, J. Y., Park, J., Nandadasa, C. N., Kim, Y., Bang, J., Lee, K., Lee, K. H., Zhang, Y., Ma, Y., *et al.* Ferromagnetic Quasi-Atomic Electrons in Two-Dimensional Electride. *Nat. Commun.* **2020**, *11*, 1–8.

(26) Hirayama, M., Matsuishi, S., Hosono, H., Murakami, S. Electrides as a New Platform of Topological Materials. *Phys. Rev. X* **2018**, *8*, 31067.

(27) Inoshita, T., Jeong, S., Hamada, N., Hosono, H. Exploration for Two-Dimensional Electrides via Database Screening and *Ab Initio* Calculation. *Phys. Rev. X* **2014**, *4*, 1–8.

(28) Zhou, J., Shen, L., Yang, M., Cheng, H., Kong, W., Feng, Y. Discovery of Hidden Classes of Layered Electrides by Extensive High-Throughput Material. *Chem. Mater.* **2019**, *31*, 1860–1868.

(29) Ma, Y., Eremets, M., Oganov, A., Xie, Y., Trojan, I., Medvedev, S., Lyakhov, A., Valle, M., Prakapenka, V. Transparent Dense Sodium. *Nature*. **2009**, *458*, 182-185.

(30) Dong, X., Oganov, A., Goncharov, A., Stavrou, E., Lobanov, S., Saleh, G., Qian, G., Zhu, Q., Gatti, C., Deringer, V., Dronskowski, R., Zhou, X., Prakapenka, V., Konôpková, Z., Popov, I., Boldyrev, A., Wang, H. A Stable Compound of Helium and Sodium at High Pressure. *Nature Chemistry*. **2017**, *9,* 440-445.

(31) Tang, H., Wan, B., Gao, B., Muraba, Y., Qin, Q., Yan, B., Chen, P., Hu, Q., Zhang, D., Wu, L., Wang, M., Xiao, H., Gou, H., Gao, F., Mao, H., Hosono, H. Metal-to-Semiconductor Transition and Electronic Dimensionality Reduction of Ca_2N Electride under Pressure. *Adv. Sci.* **2018**, *5*, 1800666.

(32) Mizoguchi, H., Muraba, Y., Fredrickson, D., Matsuishi, S., Kamiya, T., Hosono, H. The Unique Electronic Structure of Mg_2Si: Shaping the Conduction Bands of Semiconductors with Multicenter Bonding. *Angew. Chem. Int. Ed.* **2017**, *56*, 10135.

(33) Liu, C., Nikolaev, S., Ren, W., Burton. L. Electrides: a review. *J. Mater. Chem. C.* **2020**, *8*, 10551.

(34) Park, J., Hwang, J. Y., Lee, K. H., Kim, S. G., Lee, K., Kim, S. W. Tuning the Spin-Alignment of Interstitial Electrons in Two-Dimensional Y_2C Electride via Chemical Pressure. *J. Am. Chem. Soc.* **2017**, *139*, 17277–17280.

(35) Rassaerts, H., Nowotny, H., Vinek, G., Benesovsky, F. Zum System Scandium - Kohlenstoff, 1. Mitt. *Monatshefte für Chemie* **1967**, *61*, 460–468.

(36) Krikorian, N. H., Bowman, A. L., Krupka, M. C., Arnold, G. P. The Preparation and Crystal Structure of Sc_4C_3. *High Temp. Sci.* **1969**, 1, 360–366.

(37) Velikanova, T. Y., Eremenko, V. N., Artyukh, L. V., Bondar, A. A., Gordiichuk, O. V. Methods of Investigation and Properties of Powder Metallurgy Materials: Phase Diagrams of Sc-M(IV-VII)-C Systems. *Sov. Powder Metall. Met. Ceram.* **1989**, *28*, 711–718.

(38) Khazaei, M., Arai, M., Sasaki, T., Chung, C. Y., Venkataramanan, N. S., Estili, M., Sakka, Y., Kawazoe, Y. Novel Electronic and Magnetic Properties of Two-Dimensional Transition Metal Carbides and Nitrides. *Adv. Funct. Mater.* **2013**, *23*, 2185–2192.

(39) Bae, S., Espinosa-García, W., Kang, Y. G., Egawa, N., Lee, J., Kuwahata, K., Khazaei, M., Ohno, K., Kim, Y. H., Han, M. J., *et al.* MXene Phase with C_3 Structure Unit: A Family of 2D Electrides. *Adv. Funct. Mater.* **2021**, *31*, 2100009 (1–8).

(40) Hu, Q., Sun, D., Wu, Q., Wang, H., Wang, L., Liu, B., Zhou, A., He, J. MXene: A New Family of Promising Hydrogen Storage Medium. *J. Phys. Chem. A* **2013**, *117*, 14253–14260.

(41) Hu, Q., Wang, H., Wu, Q., Ye, X., Zhou, A., Sun, D., Wang, L., Liu, B., He, J. Two-Dimensional Sc_2C: A Reversible and High-Capacity Hydrogen Storage Material Predicted by First-Principles Calculations. *Int. J. Hydrogen Energy* **2014**, *39*, 10606–10612.

(42) Rietveld, H. M. The Rietveld Method. *Phys. Scr.* **2014**, *89*, 098002.

(43) Kononov, A., Kuznetsov, S., Polyakov, E. Electrorefining in Molten Salts - an Effective Method of High Purity Tantalum, Hafnium and Scandium Metal Production. *J. Alloys Compd.* **1995**, *218*, 173-176.

(44) Allred, A. Electronegativity Values from Thermochemical Data. *J. Inorg. Nucl. Chem.* **1961**, *17*, 215–221.

(45) Woomer, A. H., Druffel, D. L., Sundberg, J. D., Pawlik, J. T., Warren, S. C. Bonding in 2D Donor-Acceptor Heterostructures. *J. Am. Chem. Soc.* **2019**, *141*, 10300–10308.

(46) Druffel, D. L., Woomer, A. H., Kuntz, K. L., Pawlik, J. T., Warren, S. C. Electrons on the Surface of 2D Materials: From Layered Electrides to 2D Electrenes. *J. Mater. Chem. C* **2017**, *5*, 11196–11213.

(47) Jia, X., Shao, Q., Xu, Y., Li, R., Huang, K., Guo, Y., Qu, C., Gao, E. Elasticity-Based-Exfoliability Measure for High-Throughput Computational Exfoliation of Two-Dimensional Materials. *npj Comput. Mater.* **2021**, *7*, 1–8.

(48) Druffel, D. L., Kuntz, K. L., Woomer, A. H., Alcorn, F. M., Hu, J., Donley, C. L., Warren, S. C. Experimental Demonstration of an Electride as a 2D Material. *J. Am. Chem. Soc.* **2016**, *138*, 16089–16094.

(49) Fall, C. J., Binggeli, N., Baldereschi, A. Deriving Accurate Work Functions from Thin-Slab Calculations. *J. Phys. Condens. Matter* **1999**, *11*, 2689–2696.

(50) Biesinger, M. C., Lau, L. W. M., Gerson, A. R., Smart, R. S. C. Resolving Surface Chemical States in XPS Analysis of First Row Transition Metals, Oxides and Hydroxides: Sc, Ti, V, Cu and Zn. *Appl. Surf. Sci.* **2010**, *257*, 887–898.

(51) Merrick, J. Bonding in Scandium Monosulfide a NaCl Crystal Type, *Iowa State University*, **1980**.

(52) Barr, T. L., Seal, S. Nature of the Use of Adventitious Carbon as a Binding Energy Standard. *J. Vac. Sci. Technol. A Vacuum, Surfaces, Film.* **1995**, *13*, 1239–1246.

(53) Ramqvist, L., Hamrin, K., Johansson, G., Fahlman, A., Nordling, C. Charge Transfer in Transition Metal Carbides and Related Compounds Studied by ESCA. *J. Phys. Chem. Solids* **1969**, *30*, 1835–1847.

TOC Graphic

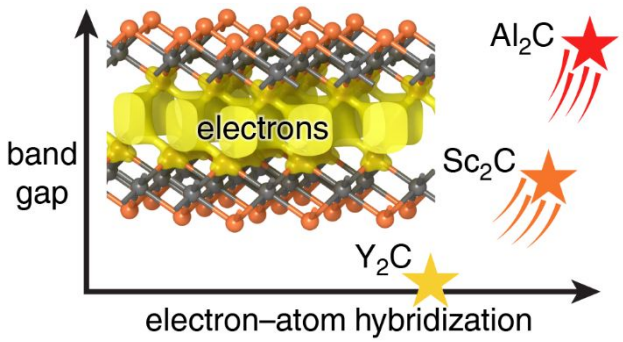
band
gap
electrons
Al_2C
Sc_2C
Y_2C
electron–atom hybridization